Available online at www.sciencedirect.com
ScienceDirect
Journal of Solid State Chemistry 180 (2007) 3288–3295
JOURNAL OF SOLID STATE CHEMISTRY
www.elsevier.com/locate/jssc

Aqueous mineralization process to synthesize uniform shuttle-like $BaMoO_4$ microcrystals at room temperature

Xueying Wu, Jin Du, Haibo Li, Maofeng Zhang, Baojuan Xi, Hai Fan, Yongchun Zhu, Yitai Qian*

Hefei National Laboratory for Physical Sciences at Microscale, Department of Chemistry, University of Science and Technology of China, Number 96, JinZhai Road, Hefei City, Anhui Province 230026, People's Republic of China

Received 24 May 2007; received in revised form 17 July 2007; accepted 18 July 2007
Available online 26 July 2007

Abstract

Single-crystalline $BaMoO_4$ microcrystals with uniform shuttle-like morphology have been successfully prepared via a facile aqueous solution mineralization process at room temperature. It was found that the pH value and the reaction temperature had important influences on the formation of the $BaMoO_4$ microcrystals. The shuttle-like microcrystals can be obtained in alkaline aqueous solution (pH = 9–14), and when the pH value was adjusted to 6–7, cocoon-like microcrystals appeared. A possible two-stage growth process has been proposed, and the Ostwald ripening was responsible for the formation of the shuttle-like $BaMoO_4$ microcrystals. The products were characterized by XRD, XPS, FESEM, HRTEM and Raman spectroscopy. Room-temperature photoluminescence indicated that the as-prepared $BaMoO_4$ microcrystals had a strong blue emission peak centered at 438 nm.

Keywords: Crystal morphology; Mineralization process; Microcrystal; Molybdates

1. Introduction

Molybdates of relatively large bivalent cations (ionic radius >0.99 Å: Ca, Ba, Pb, Sr) usually exit in the so-called scheelite structure form (scheelite = $CaWO_4$), where the molybdenum atom adopts a tetrahedral coordination [1]. Scheelite-type molybdates are reciprocally soluble over the entire compositional range [2], which results in a rich family of solid-state solution compounds. Molybdates of smaller bivalent cations $MMoO_4$ (ionic radius <0.77 Å: M = Fe, Mn, Co, Ni, Mg, Zn), however, belong to the wolframite structure (wolframite = {(Fe, Mn) WO_4}, where the molybdenum atom adopts an overall 6-fold coordination [3].

As to the $BaMoO_4$, which has two structures, namely cubic (α) and tetragonal distorted scheelite (β), depends on the applied temperature [4]. $BaMoO_4$ with the scheelite structure is one of the most important inorganic materials among the metal molybdate families, which has potential applications in various fields, such as photoluminescence (PL) and hosts for lanthanide-actived lasers [5]. Traditionally, various methods including templated synthesis [6], complex polymerization method [7], Langmuir–Blodgett technology [8], chemical vapor deposition [9], and electrochemical method [10] were applied to synthesize $BaMoO_4$ with different shapes, such as nanopowders [7], microfilms [10]. Recently, the techniques using microemulsions and reverse micelles have been used to prepare nano- or microscaled $BaMoO_4$ crystals. For example, dendritic $BaMoO_4$ microcrystals have been prepared by a microemulsion-mediated method at room temperature [11] and $BaMoO_4$ nanobelt superstructures were synthesized at a catanionic reverse-micelle system at 50 °C [12].

In recent years, a room-temperature aqueous mineralization process has been developed, which required mild reaction conditions under normal atmospheric pressure, ideally, mimicking the natural mineralogical or biological process conditions [13]. In the mineralization process, especially the technique using polymer or double

*Corresponding author. Fax: +86 551 3607402.
E-mail address: ytqian@ustc.edu.cn (Y. Qian).

0022-4596/$ - see front matter © 2007 Published by Elsevier Inc.
doi:10.1016/j.jssc.2007.07.010

hydrophilic block copolymers (DHBCS) as crystal modifiers have enriched its application in the nanoscience, as it not only generate novel superstructures but also control the nucleation and growth process [14,15]. Until now, many micro- or nanosized materials have been successfully synthesized by this technique. For example, the complex spherical $BaCO_3$ superstructures have been synthesized by a facile mineralization process with the poly (sodium 4-styrenesulfonate) (PSS) and poly (allylamine hydrochloride) (PAH) as structure-directing agents [16]. Funnel-like $BaCrO_4$ superstructures and $BaSO_4$ fiber bundles have also been prepared by polymer-controlled mineralization reactions using the sodium polyacrylate as structure-directing agents [17].

In this paper, we demonstrate a facile room-temperature aqueous solution mineralization process to prepare the uniform shuttle-like $BaMoO_4$ microcrystals without any structure-directing agent. The influences of pH value and the reaction temperature on the morphology of the as-prepared products and the growth process of the $BaMoO_4$ microstructures have been systematically investigated in such a reaction system. It was found that the alkaline aqueous solution (pH = 9–14) and room temperature (25–35 °C) were the optimal condition for the formation of the shuttle-like $BaMoO_4$ microcrystals.

2. Experiment section

All the chemicals (of analytical grade) are purchased from Shanghai Chemical Regent Company, and used without further purification.

In a typical procedure, 0.5 mmol $BaCl_2 \cdot 2H_2O$ and 0.5 mmol H_2MoO_4 were dissolved into 20 mL distilled water, respectively. After the H_2MoO_4 aqueous solution was fixed to pH value of 9 using NaOH (1 M) aqueous solution, the $BaCl_2$.aqueous solution was dripped to it under stirring for about 5 min. The reaction system was kept still and the resultant mixture was incubated for 6 h at room temperature. After that, the as-obtained white precipitate was filtered and washed with distilled water and absolute ethanol several times to remove ions possibly remnant in the final products and dried at 60 °C in air for 6 h.

The phase and purity of the products were examined by X-ray powder diffractometer using an X'Per PRD SUPER with Cu$K\alpha$ radiation ($\lambda = 1.5418$ Å). The operation voltage and current were kept at 40 kV and 40 mA, respectively. The 2θ range was 10–70° in steps of 0.02° with a count time of 2 s. The field emission scanning election microscopy (FESEM) images were taken on a JEOLJSM-6700FSEM. High-resolution TEM images were obtained using a JEOL 2010 electron microscope (200 kV). The Raman spectrum was obtained at room temperature with a LABRAM-HR Laser Micro-Raman spectrometer. The room temperature PL spectrum was performed on a Jobin Yvon-Labram spectrometer using the 370 nm excition line of the He–Cd laser.

3. Results and discussions

3.1. XRD pattern of the prepared products

Fig. 1 shows the X-ray diffraction (XRD) pattern of the as-prepared product. All the peaks can be well indexed to the tetragonal phase of $BaMoO_4$ with calculated cell constants $a = 5.569$ Å, $c = 12.794$ Å, which are in good agreement with the literature data (JCPDS card number 29-0193, $a = 5.580$ Å, $c = 12.820$ Å). No peaks of other impurities were detected, which indicated that the products had a high purity. In addition, the strong and sharp diffraction peaks also suggested the high crystallization of $BaMoO_4$ products.

3.2. Raman spectrum and XPS analysis

$BaMoO_4$ with the scheelite structure had characteristic Raman peaks due to the C_{4h}^6 or $I4_1/a$ symmetry. The Raman spectrum of the shuttle-like $BaMoO_4$ microcrystals is shown in Fig. 2a. It can be seen that there are six Raman peaks at 325, 347, 360, 792, 837, and 891 cm^{-1}, which correspond to several different vibrational modes, including $v_2(B_g)$, $v_4(B_g)$, $v_4(E_g)$, $v_3(E_g)$, $v_3(B_g)$, and $v_1(A_g)$, of the tetragonal $BaMoO_4$ crystals [18]. Obviously, the Raman spectrum also shows the well-resolved sharp peaks for the $BaMoO_4$ microcrystals, indicating that the synthesized crystals are highly crystallized.

The purity and the composition of the product were further investigated by X-ray photoelectron spectroscopy (XPS). The peak at about 780.05 eV is attributed to Ba $3d_{5/2}$ (Fig. 2b), and the peak at 231.65 eV is belonging to the Mo $3d_{5/2}$ (Fig. 2c), which are consistent with those observed in $BaMoO_4$ [10]. As shown in Fig. 2d, the O1s core-level spectrum is broad, and three Gaussians are resolved by using a curve-fitting procedure. The peak at the lower energy of 529.95 eV, is in agreement with that for O^{2-} in $BaMoO_4$ [10], while peaks at the high energies of 531.95 and

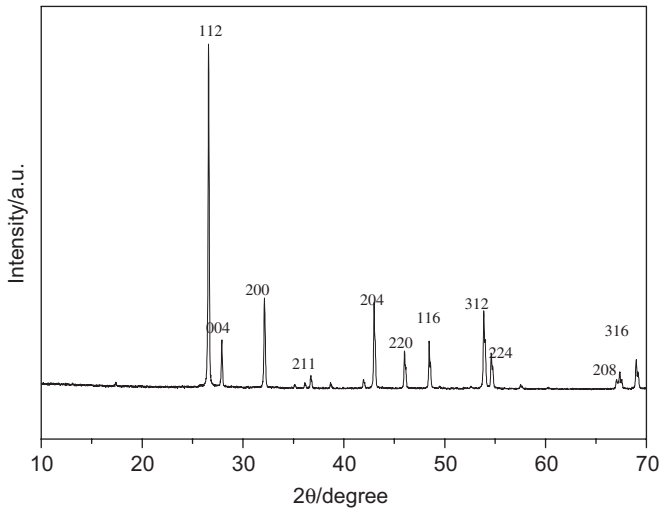

Fig. 1. XRD pattern of the as-prepared product.

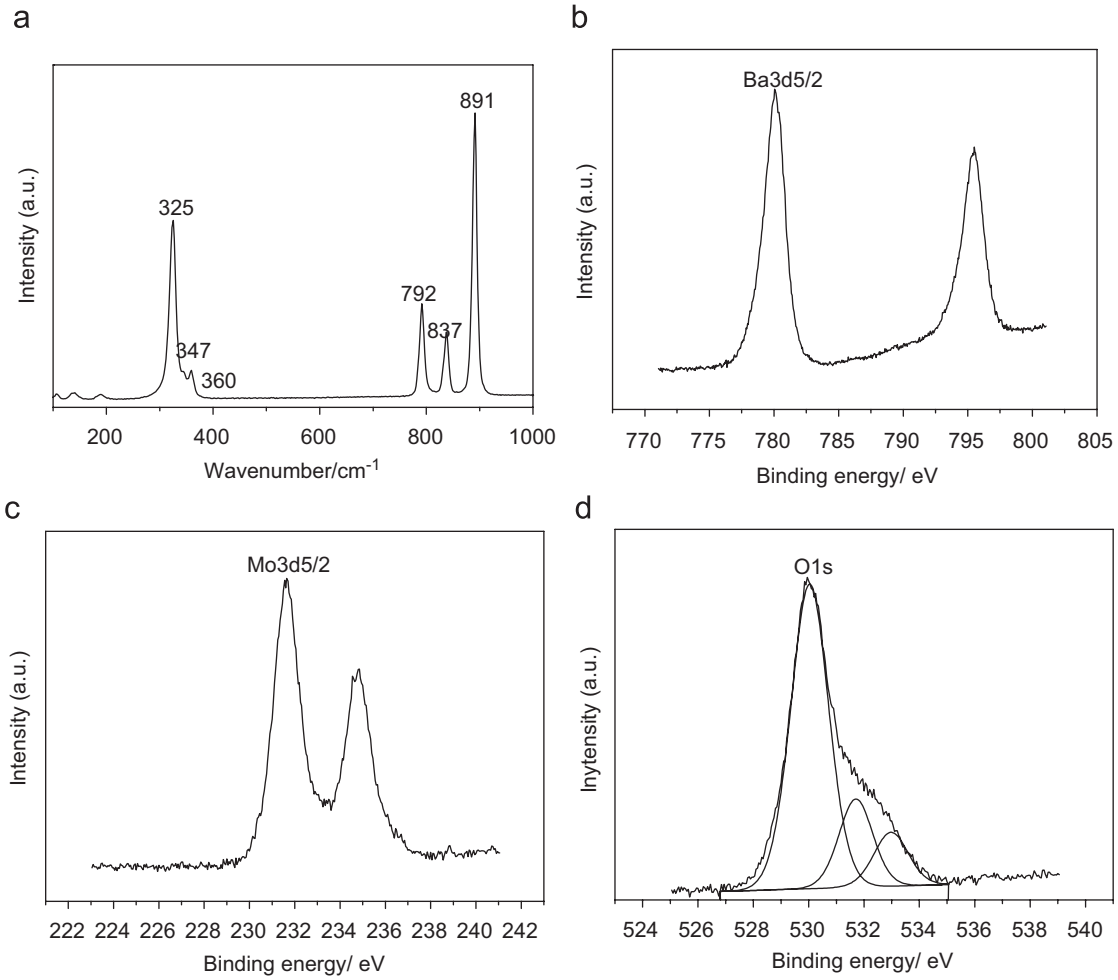

Fig. 2. (a) Raman spectra and XPS analysis; (b) for Ba element; (c) for Mo element; (d) for O element.

533.2 eV, respectively, are attributed to oxygen absorbed onto the surface of the products. Thus, the XPS results reveal the presence of Ba, Mo and O elements in the products, and confirm that the valence of Ba, Mo and O elements are +2, +6 and −2 respectively.

3.3. Morphology of the products

The morphology and dimension of the as-prepared products for 6 h (pH = 9) were examined by FESEM. Fig. 3a shows the panorama of the $BaMoO_4$ microcrystals, which consists of a large quantity of relatively uniform shuttle-like crystals with two sharp tips and four symmetrically grown protrusions in the middle, which has a typical 4-fold symmetry. It is interesting to find that they also have deep grooves between the two neighboring surfaces. A single shuttle-like $BaMoO_4$ crystal is 40–60 μm in length and 5–10 μm in width for the middle section, respectively. A HRTEM image in Fig. 3c was taken from the selected area marked in Fig. 3b, showing lattice spacing of ca. 0.513 nm, which agrees well with the separation between the {1 0 1} lattice planes of tetragonal $BaMoO_4$. The inset in Fig. 3c is selected area election diffraction (SAED) pattern of the corresponding edge of the shuttle-like $BaMoO_4$ microcrystals, which was obtained by focusing the election beam along the $[1\bar{5}1]$ axis. There a highly symmetrical dotted lattice can be seen, which reveals the single crystalline nature of the product (more ED patterns are provided in Fig. S1). Both the HRTEM image and the SAED pattern demonstrate that the shuttle-like $BaMoO_4$ microcrystals have a preferential growth orientation along the *c*-axis direction.

3.4. The reaction conditions on the formation of shuttle-like $BaMoO_4$ microcrystals

3.4.1. The influence of pH

It was found that the pH had an important role in the crystallization and shape control of $BaMoO_4$. And the alkaline aqueous solution (pH = 9–14) was the optimal condition for the formation of the shuttle-like $BaMoO_4$ microcrystals. If the pH value was lower than 6, no product can be obtained because the precipitate could dissolve in such an acidic solution When the pH of mixed aqueous solution was adjusted to 6–7, cocoon-like microcrystals with a diameter of about 500–600 nm and a length of

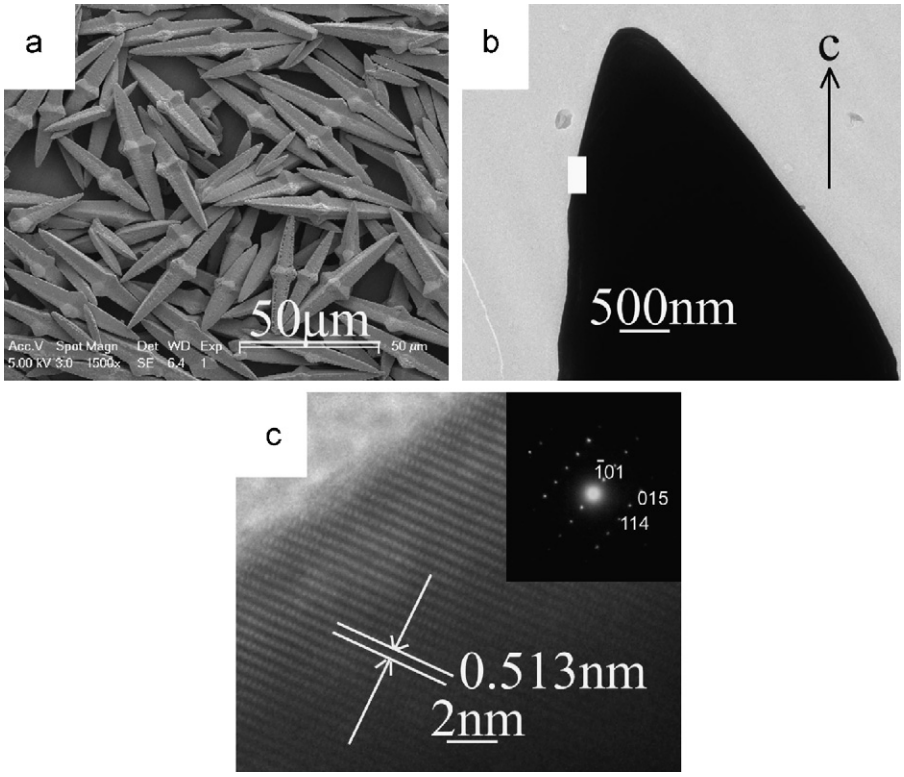

Fig. 3. (a) FESEM image of the products showing that the product contains a large quantity of shuttle-like microcrystals; (b) TEM image of a single shuttle-like $BaMoO_4$ microcrystal; (c) HRTEM image of the rim part of the microcrystal with clearly resolved lattice fringes. The inset in Fig. 3c is the SAED pattern recorded from the same microcrystal.

4–5 μm can be seen. (It has good crystallinity and the XRD pattern is shown in Fig. S2.) The SEM and TEM images for the product are shown in Fig. 4a and b, from which we can clearly see that the surface structure of the $BaMoO_4$ product is composed of irregular subunits, and the subunits assemble into such architecture.

3.4.2. *The influence of reaction temperature*

In addition, the reaction temperature also plays a key role in the formation of shuttle-like $BaMoO_4$ microcrystals. Fig. 5 shows the TEM images of products synthesized at room temperature, 50, 80 and 120 °C. And Fig. 5a is the TEM image of the product obtained at room temperature, which is consistent with the SEM image in Fig. 3a. When the reaction temperature was set at 50 °C, the morphology of the products has no obvious change with that obtained at room temperature, except that the size becomes smaller (Fig. 5b). At 80 °C, many oval-like particles with a mean length of 3 μm and a mean width of 1.5 μm were formed (Fig. 5c). And if increasing the reaction temperature to 120 °C, some cube-like particles were obtained, as shown in Fig. 5d. That is to say, with the increasing of the reaction temperature, the shuttle-like microcrystals gradually developed into particles, and this is different from the synthesis of $BaWO_4$, which experienced a morphological transform process from the shuttle-like particles to dendrites [19]. Generally, the growth habit of crystals is mainly determined by the internal structure of a given crystals and affected by external conditions such as temperature, supersaturation and so on. When the temperature is quite low, the crystal growth habit is mainly affected by the interior structure, while the temperature increases, the growth rates of different faces for the shuttle-like particles arise and the preferential growth eliminates, thus form the cube-like particles. The above results suggest that further increasing of reaction temperature does not favor the formation of shuttle-like microcrystals and the room temperature (25–35 °C) might be the optimal condition for the formation of shuttle-like $BaMoO_4$ microcrystals.

3.5. *The growth process of the $BaMoO_4$ microcrystals*

To substantially understand the growth process of the shuttle-like $BaMoO_4$ microcrystals, we had systematically surveyed the growth process by analyzing the samples at different growth stages. Fig. 7a–e shows the FESEM images for the samples taken at different stages of the aging times. The detailed growth process of the products may be described as follows: Fig. 7a was the SEM image of the products that were formed after the two mixed solutions were stirred for 10 min. The product mainly consisted of different morphologies of $BaMoO_4$ particles, such as irregular particles and some imperfect bipyramidal-like particles. It is interesting that the bipyramidal-like particles have different nucleation rates between the top section and the middle section. The top section perfectly grew, whereas

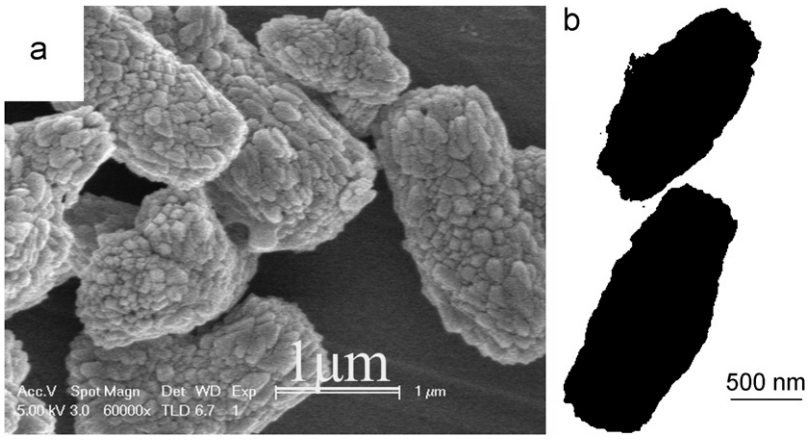

Fig. 4. FESEM images of the samples at PH = 6–7: (a) low-magnification SEM image of the products showing that the product contains a large quantity of cocoon-like materials; (b) the TEM image of the cocoon-like $BaMoO_4$ microcrystals.

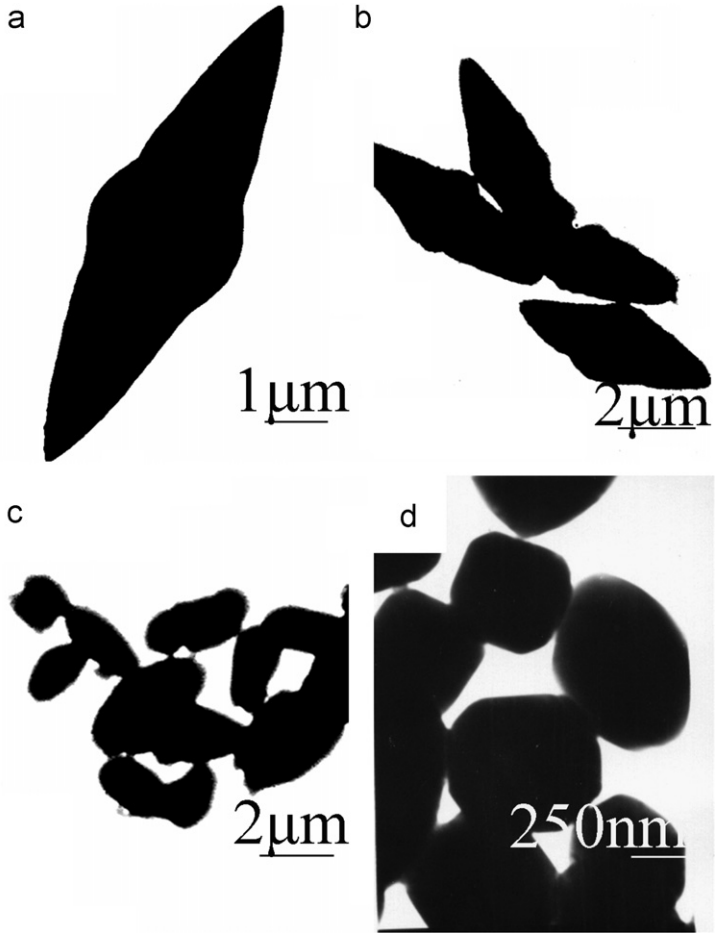

Fig. 5. The TEM images of the products at different reaction temperatures: (a) room temperature; (b) at 50 °C; (c) at 80 °C; (d) at 120 °C.

the middle section was composed of many irregular particles and led to the presence of the many interstices. When the aging time was extended to 30 min, the quantity of the irregular particles decreased gradually and more bipyramidal-like particles can be seen, but the middle section was still not compact enough to combine well with the top section, as observed from the inset of Fig. 7b. If the aging time was prolonged to 1 h, the irregular particles vanished and only the bipyramidal-like particles with a length of about 10 μm could be found. Via close examination of the Fig. 7c, it is clear that four protrusions in the middle section for the bipyramidal-like particles had come

into being and there were many holes in their faces, which might indicate that the crystallization was poor. With increasing the aging time to 3 h, there were no obvious changes for the bipyramidal-like particles except that the surfaces became smoother (shown in Fig. 7d). With the extension of the mineralization process to 6 h, perfect shuttle-like microcrystals with the deep grooves between the neighboring surfaces and four symmetrically grown protrusions in the middle were produced on a large scale. From the above results, we can find that the ratio of the length to the width of the products has become larger and better crystallization with increasing the aging time. Fig. 6 shows the XRD patterns of the products obtained at prolonged aging times, all of which can be indexed as the tetragonal phase of $BaMoO_4$. Similar diffraction peaks can be seen except that the intensity of the peaks increases.

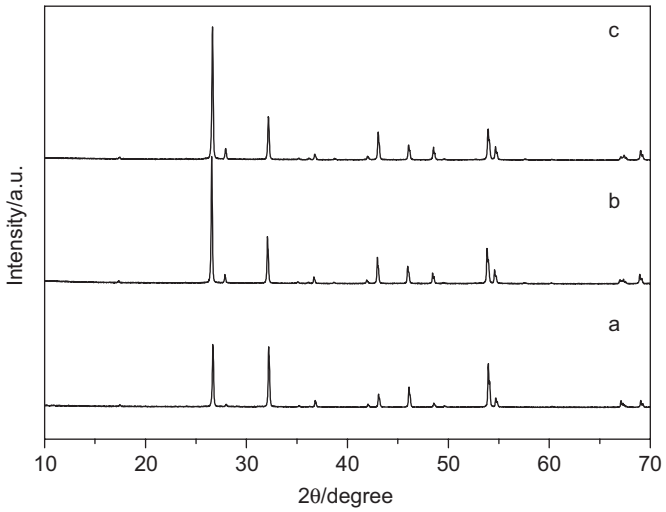

Fig. 6. The XRD patterns obtained at different aging times: (a) 10 min; (b) 1 h; (c) 3 h.

In general, two classical crystal growth modes have been often used to explain the growth process of inorganic materials: one is the so-called Ostwald ripening [20], in which the large particles grow at the cost of the small ones through the diffusion of ions, atoms, or molecules within an assemble of crystallites; another growth mode involving mostly oriented particle aggregation [21–24], which were termed conceptually as "the oriented attachment" by Penn and Banfield et al. [25–28], has emerged recently as highlighted by Allvisatos [29]. And in the experiment, the formation of cocoon-like microcrystals at pH 6–7 belongs to the oriented attachment process. In this mechanism, the

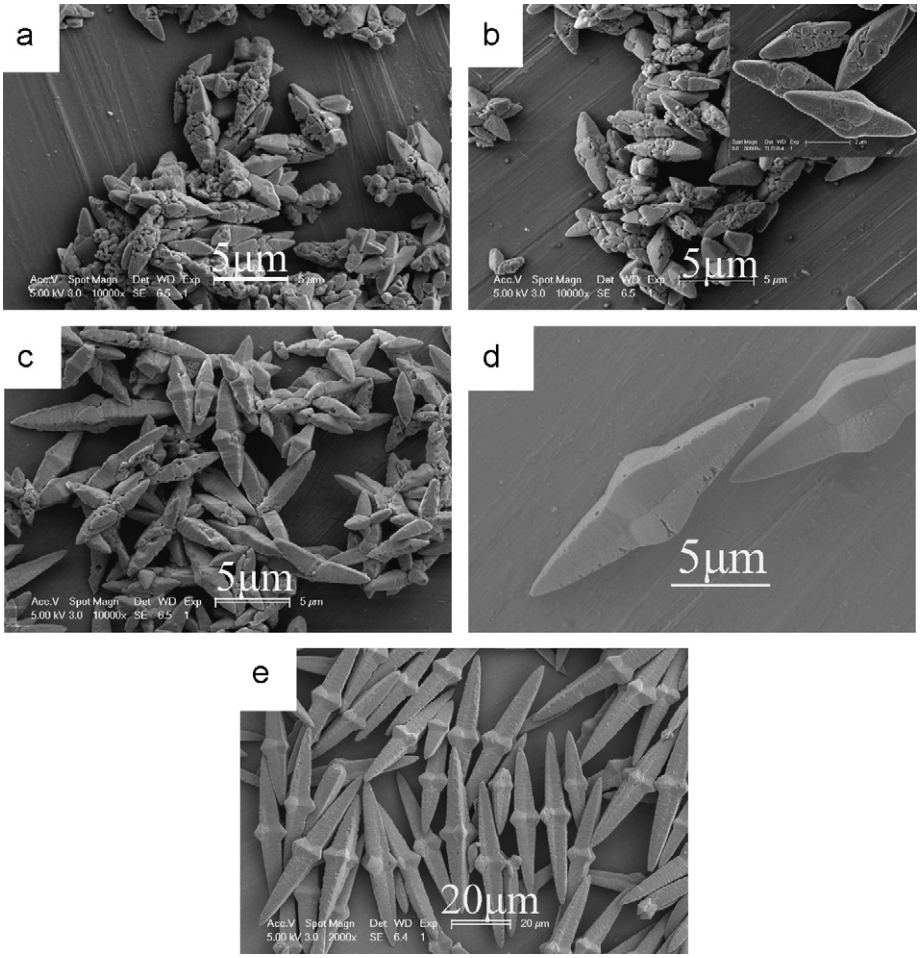

Fig. 7. FESEM images of the samples with different aging time: (a) 10 min; (b) 30 min; (c) 1 h; (d) 3 h; (e) 6 h.

bigger particles grow from small primary particles through an oriented attachment process, in which the adjacent particles are self-assembled by sharing a common crystallographic orientation and docking of these particles at a planar interface.

Based on the XRD and the FESEM measurements, we proposed that the process for the formation of the shuttle-like $BaMoO_4$ microcrystals could be divided into two stages. The first one is the formation of the perfect bipyramidal-like particles, which belongs to a typical Ostwald ripening process. When Ba^{2+} ions and MoO_4^{2-} ions were mixed, a highly supersaturated solution was formed, leading to the coexistence of the irregular particles and the bipyramidal-like $BaMoO_4$ particles, as shown in Fig. 7a. It is clear that the crystalline phase of the nuclei is critical for directing the intrinsic shapes of the crystals due to its characteristic symmetry and structure. As the aging time proceeded, the bipyramidal-like particles became predominating in the products via a transformation process using the irregular particles as precursors. The formation process of the bipyramidal-like particles is shown in Fig. 8 (Stage 1).

The second stage is the evolution process from the bipyramidal-like particles to the shuttle-like microcrystals. Fig. 8 (Stage 2) is the schematic illustration of the formation of the shuttle-like $BaMoO_4$ microcrystals evolved from the bipyramidal-like particles. The newly grown nuclei first grew into bipyramidal-like particles, and then shuttle-like $BaMoO_4$ microcrystals with excellent symmetry were formed with further growth of bipyramidal-like particles, which is mainly a kinetically controlled process. In addition, reduction of surface energy is the primary driving force for the crystal growth and morphology evolution. From the FESEM images, it was reasonable to presume that the bipyramidal-like particles have two growth directions along *c*- and *a*-axis. Meanwhile, just because of the nonequilibrium growth rates of the two directions, the growth rates of the former was larger than that of the latter, resulting in the appearance of the deep grooves between the neighboring faces. Finally, shuttle-like microcrystals were obtained. And the structure of shuttle-like microcrystals further confirmed that the microcrystals had a preferential growth orientation along the *c*-axis direction.

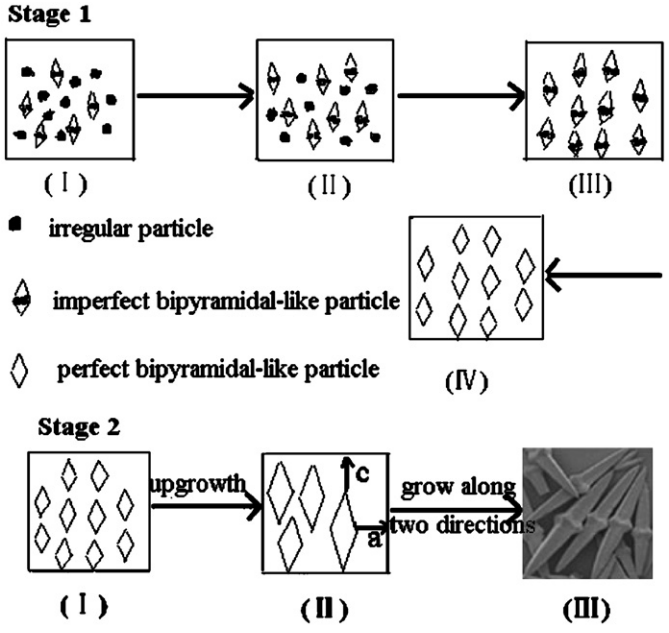

Fig. 8. Schematic illustration of the formation process of the shuttle-like $BaMoO_4$ microcrystals. Stage 1: the formation of the perfect bipyramidal-like particles through the Ostwald ripening process (I) the coexistence of the irregular particles and the bipyramidal-like particles (II) the quantity of bipyramidal-like particles increased at the cost of the small particles (III) the only presence of the bipyramidal-like particles and (IV) the perfect bipyramidal-like particles. Stage 2: the evolution process from the bipyramidal-like particles to the obtained shuttle-like $BaMoO_4$ microcrystals.

3.6. PL spectrum

The PL spectrum of the as-synthesized product was investigated at room temperature. As shown in Fig. 9,

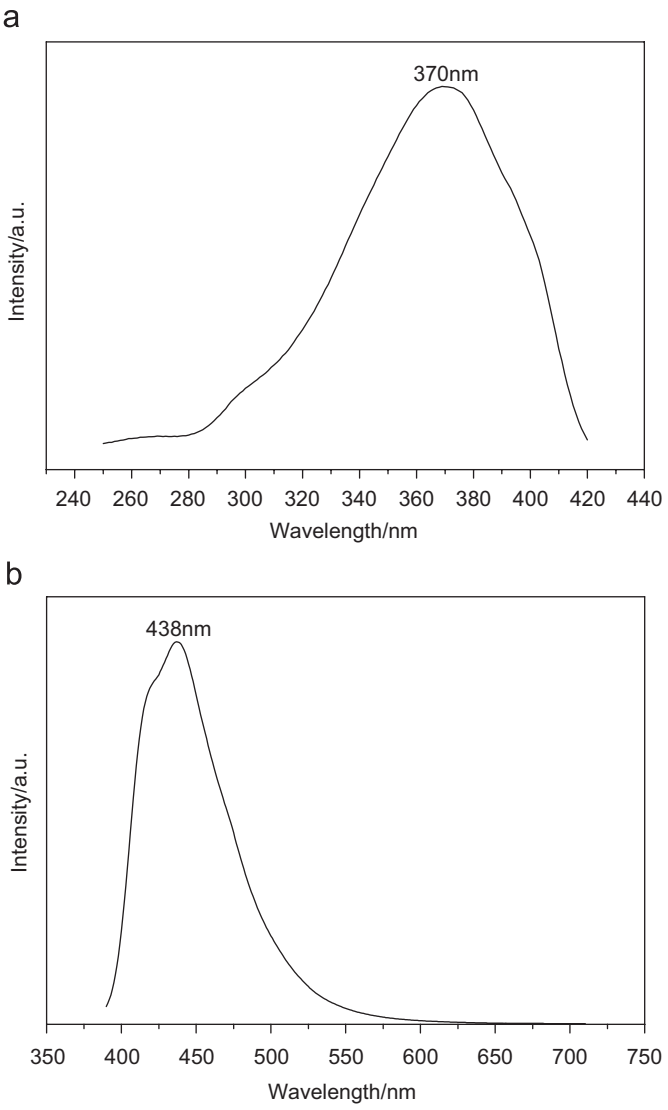

Fig. 9. Room temperature photoluminescence spectra of the shuttle-like $BaMoO_4$ microcrystals: (a) excitation spectra; (b) emission spectra.

$BaMoO_4$ microcrystals display a strong blue emission peak in the range of 400–600 nm, centered around 438 nm when excited at 370 nm, The spectral characteristic of $BaMoO_4$ was also very similar to those of the other scheelite molybdate crystals ($MMoO_4$, $M = Ca$, Sr, Pb) [30]. The emission band shape might be explained by considering the Jahn-Teller active vibration modes of T_2 symmetry that influences the $[MoO_4]^{2-}$ complex anion of slightly distorted tetrahedral symmetry, leading to a structured absorption band for the $A_1 \rightarrow T_{1(2)}$ transition [31–33]. The strong luminescence intensity indicated the perfection of the microstructure and good crystallization, since the optical property of the $BaMoO_4$ is comparable with that of the previously reported $BaMoO_4$ particles [7] that were obtained by complex polymerization method.

4. Conclusions

In summary, shuttle-like $BaMoO_4$ microcrystals were successfully prepared by a simple aqueous solution mineralization process without the assistance of any structure-directing agent at room temperature. The influences of pH value, the reaction temperature and the growth process were examined in detail. In addition, the optical properties of products had been examined by Raman spectrum and PL spectrum. Furthermore, the feasibility and ease of this synthesis route are worth exploring for other inorganic systems, since it is an efficient and facile solution-based method with promising advantages compared with the traditional high-temperature approach.

Acknowledgments

This work is financially supported by the National Natural Science Foundation of China (No. 20431020) and the 973 Project of China (No. 2005CB623601).

Appendix A. Supporting Information

Supplementary data associated with this article can be found in the online version at doi:10.1016/j.jssc.2007.07.010.

References

[1] B.G. Hyde, S. Andersson, Inorganic Crystal Structure, Wiley, New York, 1989.
[2] V.D. Zhuravlev, M.Y. Khodos, Y.A. Velikodnyi, Russ. J. Inorg. Chem. 39 (1994) 464.
[3] S.H. Yu, B. Liu, M.S. Mo, J.H. Huang, X.M. Liu, Y.T. Qian, Adv. Funct. Mater. 13 (2003) 639.
[4] T.T. Basiev, A.A. Sobol, Y.U.K. Voronko, P.G. Zverev, Opt. Mater. 15 (2000) 205.
[5] J.H. Ryu, J.W. Yoon, C.S. Lim, K.B. Shim, Mater. Res. Bull. 40 (2005) 1468.
[6] M. Wirtz, M. Parker, Y. Kobayashi, C.R. Martin, Chem. Eur. J. 8 (2002) 3572.
[7] A.P.A. Marques, D.M.A. Melo, C.A. Paskocimas, P.S. Pizani, M.R. Joya, E.R. Leite, E. Longo, J. Solid State Chem. 179 (2006) 673.
[8] F. Kim, S. Kwan, J. Akana, P.D. Yang, J. Am. Chem. Soc. 123 (2000) 4360.
[9] J.P. Ge, Y.D. Li, Adv. Funct. Mater. 14 (2004) 157.
[10] J. Bi, D.Q. Xiao, D.J. Gao, P. Yu, G.L. Yu, W. Zhang, J.G. Zhu, Cryst. Res. Technol. 38 (2003) 938.
[11] Q. Gong, X.F. Qian, H.L. Cao, W.M. Du, X.D. Ma, M.S. Mo, J. Phys. Chem. B 110 (2006) 19295.
[12] H.T. Shi, L.M. Qi, J.M. Ma, N.Z. Wu, Adv. Funct. Mater. 15 (2005) 442.
[13] Y. Xia, P. Yang, Y. Sun, Y. Wu, B. Mayers, B. Gates, Y. Yin, F. Kim, H. Yan, Adv. Mater. 15 (2003) 353.
[14] H. Colfen, S. Mann, Angew. Chem. Int. Ed. 42 (2003) 2361.
[15] S.H. Yu, H. Colfen, J. Mater. Chem. 14 (2004) 2124.
[16] S.H. Yu, H. Colfen, A.W. Xu, W.F. Dong, Cryst. Growth Design 4 (2004) 33.
[17] S.H. Yu, M. Antonietti, H. Colfen, J. Hartmann, Nano Lett. 3 (2003) 379.
[18] C.T. Xia, V.M. Fuenzalida, R.A. Zarate, J. Alloys Compd. 316 (2001) 250.
[19] X.M. Wang, H.Y. Xu, H. Wang, H. Yan, J. Cryst. Growth 284 (2005) 260.
[20] T. Sugimoto, Adv. Colloid Interface Sci. 28 (1987) 65.
[21] J.K. Bailey, C.J. Brinker, M.L. Mecartney, J. Colloid Interface Sci. 157 (1993) 1.
[22] V. Privman, D.V. Goia, J. Park, E. Matijevic, J. Colloid Interface Sci. 213 (1999) 36.
[23] A. Chemseddine, T. Moritz, Eur. J. Inorg. Chem. (1999) 235.
[24] G.J. Zhou, M.K. Lu, F. Gu, D. Xu, D.R. Yuan, J. Cryst. Growth 276 (2005) 577.
[25] R.L. Penn, J.F. Baneld, Science 281 (1998) 969.
[26] R.L. Penn, J.F. Baneld, Geochim. Cosmochim. Acta 63 (1999) 1549.
[27] J.F. Baneld, S.A. Welch, H. Zhang, T.T. Ebert, R.L. Penn, Science 289 (2000) 751.
[28] R.L. Penn, A.T. Stone, D.R. Veblen, J. Phys. Chem. B 105 (2001) 4690.
[29] A.P. Alivisatos, Science 289 (2000) 736.
[30] M. Nikl, P. Bohacek, E. Mihokova, M. Kobayashi, M. Ishii, Y. Usuki, V. Babin, A. Stolovich, S. Zazubovich, M. Bacci, J. Lumin. 87 (2000) 1136.
[31] Y. Toyozawa, M. Inoue, J. Phys. Soc. Jpn. 21 (1966) 1663.
[32] Z.D. Lou, J.H. Hao, M. Cocivera, J. Lumin. 99 (2002) 349.
[33] K. Polak, M. Nikl, K. Nitsch, M. Kobayashi, M. Ishii, Y. Usuki, O. Jarolimek, J. Lumin. 72 (1997) 781.